


RESEARCH

Open Access



Generalized antenna sequence spatial modulation (GASSM): a novel framework for enhanced PHY layer security and energy efficiency

Joseph A. Obadha^{1*} , Peter O. Akuon¹ and Vitalis K. Oduol¹

*Correspondence:
joseph.obadha@gmail.com

¹Electrical and Information
Engineering, University
of Nairobi, P.O Box, 30197-00100,
Nairobi, Kenya

Abstract

In antenna sequence spatial modulation (ASSM), the spatial and symbol domains are both used to encode information. The sequencing of the antennas' transmissions within given time slots and the symbol carried in those time slots represent information in the spatial and symbol domains, respectively. The receiver's task is to decode this sequence of transmission and to detect the symbol carried in the time slots, equal to the number of antennas. For better energy efficiency and greater security, we propose a generalized ASSM, GASSM. In the GASSM, while the information is contained in both the sequence and the symbols transmitted, different symbols can be transmitted within the time slots forming the frame. This expands the code domain since the symbol and the spatial information represent a longer code in the mapper table. As a special case, we present the case of three transmit antennas, transmitting within three time slots. A combination of the antennas' sequence and the symbol carried in the time slots is used as a code for a bit sequence. Results obtained from simulation and analysis of the bit error rate performance and secrecy capacity are contrasted and presented. Comparing the GASSM to the standard spatial modulation (SM) and the ASSM, we deduce that the GASSM has a higher secrecy capacity and higher energy efficiency per bit and unlike conventional SM allows utilization of odd number of antennas.

Keywords: ASSM, SM, Security capacity, Physical layer security

Introduction

The main drivers of research into future wireless technologies are the requirement for high data rates, high reliability, security, energy efficiency and ease of implementation of the technologies in the wireless networks [1]. In any implementation, there is always need for a trade-off amongst these metrics. To improve the data rate and spectral efficiency, space modulation techniques are the leading candidates [1]. The simplest form of space modulation is the space shift keying (SSK), which employs a multiple-input–multiple-output (MIMO) approach but only activate one transmit antenna at a time and implicitly transmit information based on the antenna index that is active at that time [2].

The spectral efficiency of SSK, given by $\{\log_2\{N_t\}\}$, is quite low in spite of its simplicity. An improvement over the SSK is the generalised SSK (GSSK), in which multiple antennas can transmit simultaneously and the spectral efficiency is increased to $\left\{\left\lfloor\left(\frac{N_t}{N_u}\right)\right\rfloor\right\}$ with N_t being the total number of transmit antennas and N_u the number of antennas chosen to transmit at any given time [3].

With the use of spatial modulation (SM), which carries information in both the spatial and signal domains while only utilizing one antenna at a time to broadcast data, the spectral efficiency of transmission is further increased [4]. The spectral efficiency of the SM is given by $\{\log_2 M + \log_2 N_t\}$, where M is the modulation order. In generalised SM (GSM), a signal may be sent simultaneously by more than one antenna. This results in a spectral efficiency of $\left\{\log_2 M + \left\lfloor\left(\frac{N_t}{N_u}\right)\right\rfloor\right\}$, which is an improvement over that of conventional SM [5]. For multiple active SM (Ma-SM), the spectral efficiency is further improved to $\left\{N_u \log_2 M + \left\lfloor\left(\frac{N_t}{N_u}\right)\right\rfloor\right\}$ [6, 7].

Quadrature spatial modulation (QSM) extends the transmitted symbol into the in-phase and quadrature domains, which improves spectral efficiency [7]. With this modulation scheme, the index bits are double the length of that in the conventional SM, and the resulting spectral efficiency is determined from $\{\log_2 M + \log_2(N_t)^2\}$. To further improve on the spectral efficiency, a generalised QSM scheme was proposed, where more than one transmit antenna is activated in the in-phase and quadrature domains [8]. Other techniques such as code index modulation, where data are transmitted via direct sequence spectrum, have been proposed. In [9], the spreading code index serves as an information carrier. This raises the system's total efficiency to $\{\log_2 M + 2 \log_2 N_t\}$. This is equal to that of the QSM but higher than that of the conventional SM. However, the overall receiver hardware complexity is reduced as compared to that of conventional SM or the QSM. With this, the index bits are double the length of that in the conventional SM, and the resulting spectral efficiency is determined from $\{\log_2 M + \log_2(N_t)^2\}$.

The potential of representing the information in more than two domains has also been investigated by researchers as a way of further increasing the spectral efficiency. In [10], a third domain, the waveform domain, in addition to the spatial and signal domains, has been proposed to convey the information. In this scheme, orthogonal waveforms are used and the role of the receiver is not only to decode the symbol, which was transmitted by an antenna, but also the waveform used to carry the information. The total number of mapped bits per channel use is obtained from $\{\log_2 M + \log_2 M_c + \log_2 N_t\}$ where M_c is the number of orthogonal waveforms used. In [11], the authors explore adaptive generalized spatial modulation (AGSM), where it is demonstrated that, for the same level of spectral efficiency, AGSM requires fewer antennas than GSM. An innovative implementation of adaptive SM, the layered baud space modulation, (LSM), is proposed in [12]. Unlike the conventional SM where only a single antenna transmits in a baud space, in LSM, asynchronous layered transmission by multiple antennas, M_a , is allowed within a time slot. This gives a spectral efficiency of $\{M_a + \log_2(M^{N_a})\}$ where M_a is the number of active antennas and M is the modulation order.

A trade-off of spectral efficiency and secrecy capacity has been explored in [13]. An innovative system is suggested by the authors of this study of achieving a higher secrecy

capacity albeit at a reduced spectral efficiency and is given by $\frac{1}{3} \{ \log_2 M + \log_2 N_t \}$. In this proposed method, the ASSM, information is carried in both the signal domain and the spatial domain. Spatially, the information is implicitly carried in the sequence in which the antennas transmit the information. Multiple antennas transmit the same symbol in succession, and the order in which they transmit the symbol and the symbol itself carries the information.

The ASSM is based on the novel communication methods patented in [14]. In this patent, innovative communication techniques are proposed where information is contained in the spatial and symbol domains. Specifically, in the spatial domain, the order in which the transmitting elements use the available time slots conveys the information. The constellation symbols embedded in the antennas/elements that have transmitted in that sequence are decoded for full recovery of the information. The proposed methods in this patent have physical security built in them. There are several research directions that have been explored based on this patent, and the patent in [15] to enhance various metrics of data transmission [16–20].

In [15], the authors propose a transmission technique in which the code set to be communicated is entirely encoded by a combination of antennas that transmit at a specific time instant. The signals received from the antennas therefore represent a coded information whose mapping table is available to both the transmitter and the receiver. To intercept the information, the intruder needs to know the rules of the mapping.

The authors of [16] discuss an architecture in which the information is implicitly carried in the spatial domain by the sequence in which the antennas transmit. Based on the patent of [14] a novel transmission scheme, the spatial MIMO rank modulation (SMRM), has been proposed [17]. In this scheme, the transmitting antennas are divided into ranks, which are subsets of varied sizes. Each rank is associated with a certain group of bits. For a group of bits being transmitted, the transmitter represents a group of such bits with a certain number of radio paths by choice of the number of active antennas that needs to transmit. At the receiver, the number of active radio paths is determined to decode the information which was transmitted. A part from conveying the information, the method also serves the dual purpose of offering a physical layer security because for the information to be recovered, the receiver needs complete rank decoding knowledge. The use of different ranks of carrier frequencies is discussed in [18]. It is also possible to transmit via spatial domain only by use of Gaussian channels as discussed in [19].

Shannon defined the perfect secrecy criterion [21] and suggested the information theoretic metric for secrecy systems, which prevents an observer from extracting any information from the transmit signal. It was Shannon who conducted the first formal research on physical layer security. According to Wyner's wiretap channel model, the secrecy capacity is the maximum transmission rate feasible when eavesdroppers channel observation is noisier than the genuine user channel [22, 23]. Csiszar et al [24] expanded Wyner's result to a nonzero secrecy capacity as illustrated in Fig. 2. The model contains a passive listener named Eve, a legitimate receiver named Bob, and a transmitter named Alice. Bob and Eve receive Alice's communications through separate channels. Although the essential basis for the early study on the physical layer was channel defects and jamming, a more modern channel independent protocol based on coding, called *iJAM*, has

been proposed [25, 26]. Techniques such as spread-spectrum (SS) watermarking have also been used to create physical layer security [27, 28]. A novel technique for deriving the secrecy capacity from the bit error rate has been discussed and derived by the authors in [19].

In the proposed GASSM, we show that the secrecy capacity of the ASSM and the spectral efficiency have been enhanced. We also show that the bit error rate has been improved, compared to that of the conventional SM. We employ mutual information and sample variance techniques introduced in [7, 29] for the investigation of the BER and the secrecy capacity performance.

Motivations and contributions

1. The GASSM, a novel transmit antenna sequence-based communication strategy that improves on the ASSM, is presented as a new communication paradigm;
2. Analytical methods and simulation framework are developed for the analysis of the BER of the system;
3. From the analytical BER expressions, a novel method of obtaining the secrecy capacity of the proposed communication method is presented;
4. The simulated results of the proposed system are compared with those of the conventional spatial modulation and the ASSM schemes.

Organisation and notation

The rest of the paper is arranged as follows: “[Proposed system model of the GASSM](#)” section discusses the proposed GASSM system model. This includes the signal transmission and detection, the detection complexity, mapping table for various implementations of the model and a discussion of the correlated channel model. “[Error performance Analysis](#)” section covers the error performance analysis. We give an overview of the sample variance (SV) and mutual information (MI) criterion adopted for bit error analysis in this paper. “[Secrecy rate analysis](#)” section discusses the secrecy rate and the derivation of secrecy capacity from bit error rate. Discussion of the results and the conclusion are presented in Sects. [Results and Analsis](#) and [Conclusion](#)” sections, respectively.

Column vectors and matrices, respectively, are denoted by lower- and upper-case boldface characters. \mathbb{C} stands for the complex number field, whereas $(\cdot)^T$ and $(\cdot)^H$ stand for the transpose and Hermitian transpose operations, respectively. An identity matrix of size $M \times M$ is represented as \mathbf{I}_M . The Frobenius norm and binomial operations are indicated by $\|\cdot\|$ and $\mathbf{C}(\cdot, \cdot)$, respectively. $\mathbf{R}\{\cdot\}$ and $\mathbf{I}\{\cdot\}$ represent the real and imaginary parts of a variable, respectively. The Gaussian Q -function is represented by $\mathbf{Q}(\cdot)$.

Proposed system model of the GASSM

The proposed system model for the GASSM is shown in Fig. 1. The bit splitter splits the incoming block of bits into two parts: the first part determines the antenna sequence of transmission within the three time slots, and the second part selects the bits to be transmitted in each of the antennas with each antenna conveying one bit per time slot. As an example, consider the expanded 7 bit-GASSM encoder in Table 1.

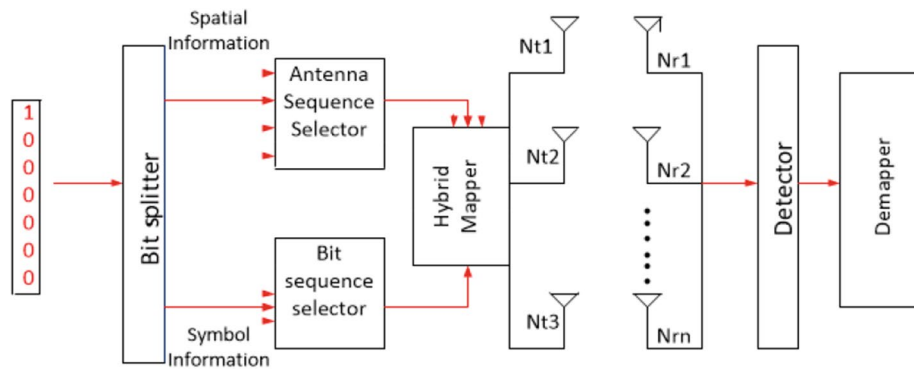


Fig. 1 Proposed GASSM system

Table 1 GASSM mapping Table: 7 bit BPSK transmission, symbol x

GASSM/index	Tx antenna		
	TS_1	TS_2	TS_3
1	a_1x_1	a_1x_1	a_1x_1
2	a_1x_1	a_1x_1	a_1x_2
3	a_1x_1	a_1x_2	a_1x_1
4	a_1x_1	a_1x_2	a_1x_2
5	a_1x_2	a_1x_1	a_1x_1
6	a_1x_2	a_1x_1	a_1x_2
7	a_1x_2	a_1x_2	a_1x_1
8	a_1x_2	a_1x_2	a_1x_2
⋮	⋮	⋮	⋮
121	a_3x_1	a_2x_1	a_2x_1
122	a_3x_1	a_2x_1	a_2x_2
123	a_3x_1	a_2x_2	a_2x_1
124	a_3x_1	a_2x_2	a_2x_2
125	a_3x_2	a_2x_1	a_2x_1
126	a_3x_2	a_2x_1	a_2x_2
127	a_3x_2	a_2x_2	a_2x_1
128	a_3x_2	a_2x_2	a_2x_2

Table 2 GASSM mapping Table: 7 bit BPSK transmission, symbol x

GASSM/index	TS_1		TS_2		TS_3	
	Ant	symbol	Ant	symbol	Ant	symbol
1	1	1	1	1	1	1
2	1	1	1	1	1	-1
3	1	1	1	-1	1	1
4	1	1	1	-1	1	-1
⋮	⋮	⋮	⋮	⋮	⋮	⋮
127	3	-1	2	-1	2	1
128	3	-1	2	-1	2	-1

The table shows which antenna transmits which symbol in which time slot. For example, index 1 is represented by antenna a_1 transmitting the symbol x_1 in all the three time slots. Table 2 shows the expanded version of Table 1 where the actual BPSK symbols transmitted are shown. GASSM index 1 is represented with the bit pattern 0000001.

The bit pattern would be split so that the four bit binary pattern 1000 is sent to the antenna sequence selector, which uses it to decode the antenna sequence, which, according to the table, turns out to be 111. This implies that in the next three time slots, only antenna 1 will be used to transmit the data at intervals of a time slot. That means antenna 1 transmits in time slots 1, 2 and 3. The remaining three bits 000 are simultaneously fed to the bit sequence selector and choose one of the possible permutations of the 3 bit pattern of the BPSK symbol. In this instance, the 000 is associated with the sequence 111.

The hybrid mapper simultaneously uses the information from the antenna sequence selector and the bit sequence selector to map the bits to the appropriate antennas. The signal is picked up at the receiver via a number of antennas. The transmitted bit pattern can be recovered by passing the received signal through the detector and, eventually, to a corresponding demapper.

Table 3 shows the GASSM mapping for 6-bit 4-QAM transmission. For example, in row 1, antenna 1 (a_1) transmits a QAM symbol (x_1) in all the three time slots. Table 4 is an expansion of Table 3 showing the actual symbols carried by the antennas. Similarly, Table 5 shows the GASSM mapping for the 5-bit BPSK mapping and its expansion in Table 6.

At the detection stage, the GASSM system can be considered to be operating as multiactive SM (MA-SM) system. The detector operates per time slot, by detecting the antenna that transmitted in a given time slot and the symbol carried by that

Table 3 GASSM mapping Table: 6 bit 4-QAM Transmission, symbol x

GASSM/index	Tx antenna		
	TS_1	TS_2	TS_3
1	a_1x_1	a_1x_1	a_1x_1
2	a_1x_2	a_1x_2	a_1x_2
3	a_1x_3	a_1x_3	a_1x_3
4	a_1x_4	a_1x_4	a_1x_4
5	a_1x_1	a_1x_1	a_2x_1
6	a_1x_2	a_1x_2	a_2x_2
7	a_1x_3	a_1x_3	a_2x_3
8	a_1x_4	a_1x_4	a_2x_4
⋮	⋮	⋮	⋮
57	a_3x_1	a_3x_1	a_2x_1
58	a_3x_2	a_3x_2	a_2x_2
59	a_3x_3	a_3x_3	a_2x_3
60	a_3x_4	a_3x_4	a_2x_4
61	a_3x_1	a_2x_1	a_2x_1
62	a_3x_2	a_2x_2	a_2x_2
63	a_3x_3	a_2x_3	a_2x_3
64	a_3x_4	a_2x_4	a_2x_4

Table 4 Expanded GASSM mapping Table: 6 bit 4-QAM Transmission, symbol x

GASSM/index	TS_1		TS_2		TS_3	
	Ant	Symbol	Ant	Symbol	Ant	Symbol
1	1	$(+1 + j)$	1	$(+1 + j)$	1	$(+1 + j)$
2	1	$(-1 + j)$	1	$(-1 + j)$	1	$(-1 + j)$
3	1	$(-1 - j)$	1	$(-1 - j)$	1	$(-1 - j)$
4	1	$(+1 - j)$	1	$(+1 - j)$	1	$(+1 - j)$
⋮	⋮	⋮	⋮	⋮	⋮	⋮
63	3	$(-1 - j)$	2	$(-1 - j)$	2	$(-1 - j)$
64	3	$(+1 - j)$	2	$(+1 - j)$	2	$(+1 - j)$

Table 5 GASSM mapping Table: 5 bit BPSK transmission, symbol x

GASSM / Index	Tx Antenna		
	TS_1	TS_2	TS_3
1	a_1x_1	a_1x_1	a_1x_1
2	a_1x_2	a_1x_2	a_1x_2
3	a_1x_1	a_1x_1	a_2x_1
4	a_1x_2	a_1x_2	a_2x_2
⋮	⋮	⋮	⋮
28	a_3x_1	a_3x_1	a_2x_1
29	a_3x_2	a_3x_2	a_2x_2
31	a_3x_1	a_2x_1	a_2x_1
32	a_3x_2	a_2x_2	a_2x_2

Table 6 Expanded GASSM mapping Table: 5 bit BPSK transmission, symbol x

GASSM/index	TS_1		TS_2		TS_3	
	Ant	symbol	Ant	symbol	Ant	symbol
1	1	1	1	1	1	-1
2	1	-1	1	-1	1	-1
3	1	1	1	1	2	1
4	1	-1	1	-1	2	-1
⋮	⋮	⋮	⋮	⋮	⋮	⋮
31	3	1	2	1	2	1
32	3	-1	2	-1	2	-1

antenna. After three consecutive time slots. The received patterns are decoded to obtain the bit pattern that was transmitted.

Signal model

The signal vector at the receiver can be expressed in the form of:

$$y_k = Hx_k + n_k \tag{1}$$

where k denotes the time slot and $k \in [1 : N_t]$ and \mathbf{y} and \mathbf{n} , respectively, are vectors of received signal and additive noise each element being an i.i.d complex Gaussian random variable (RV) with the distribution $CN(0, \sigma_N^2)$. The matrix \mathbf{H} represents a frequency flat Rayleigh fading channel's transfer function, which is completely known at the receiver. \mathbf{x}_k is the transmitted vector of the k^{th} time slot. For each value of k , the received signal is independently decoded and demapped using the look-up table.

Spatial correlation

The separation distance between the antennas significantly affects the channel correlation. We apply the Kronecker correlation model [30] given by:

$$\hat{\mathbf{H}} = \Sigma_r^{\frac{1}{2}} \mathbf{H}_f \Sigma_t^{\frac{1}{2}} \tag{2}$$

with Σ_r and Σ_t , respectively, representing the spatial covariance at the receiver and transmitter. \mathbf{H}_f is a $N_r \times N_t$ complex Gaussian coefficients.

$$\mathbf{H}_f = \begin{bmatrix} h_{11} & \cdots & h_{1N_t} \\ h_{21} & \cdots & h_{2N_t} \\ \vdots & \ddots & \vdots \\ h_{N_r 1} & \cdots & h_{N_r N_t} \end{bmatrix} \tag{3}$$

Since we only consider arbitrary correlation at the transmit antenna, Σ_r is taken to be an identity matrix, and Eq. (2) reduces to:

$$\hat{\mathbf{H}} = \mathbf{H}_f \Sigma^{\frac{1}{2}} \tag{4}$$

The normalised correlation matrix Σ is given by:

$$\Sigma = \begin{pmatrix} 1 & \rho_{12} & \cdots & \rho_{1N_r} \\ \rho_{21} & 1 & \cdots & \rho_{2N_r} \\ \vdots & \vdots & \ddots & \vdots \\ \rho_{N_r 1} & \rho_{N_r 2} & \cdots & 1 \end{pmatrix} \tag{5}$$

Therefore, we model the correlated channels through the well-known formula, where the correlation coefficients are derived from $\rho = J_0 \left[2\pi \left(\frac{d}{\lambda} \right) \right]$ where d is the spacing between the antennas and λ is the wavelength of the carrier [31, 32]. As an illustration, consider the case of three evenly spaced receive antennas with an antenna separation of $d = 0.1\lambda$. The normalized positive-definite correlation matrix, consisting of various correlation coefficients, ρ , is then determined to be:

$$\Sigma = \begin{pmatrix} 1 & 0.9037 & 0.6425 \\ 0.9037 & 1 & 0.9037 \\ 0.6425 & 0.9037 & 1 \end{pmatrix} \tag{6}$$

The investigations examine different antenna spacings.

Signal detection in joint space

The ML MA-SM detector [6] is used at the receiver to both detect the modulation symbol vector $x_{\hat{k}}$ and the transmit index \hat{v} , where $\hat{v}, k \in (1 : N_t)$. These are jointly detected at the receiver using the ML MA-SM detector, and this can be written as:

$$[\hat{v}, x_{\hat{k}}] = \arg \max_{(v,k)} P\{y | \hat{H}, x_{vk}\} \tag{7}$$

$$= \arg \min_{(v,k)} \left\{ \|y - \hat{H}x_{vk}\|_F^2 \right\} \tag{8}$$

where the expression of the conditional pdf of y given \hat{H} and x_{vk} is:

$$P(y | \hat{H}, x_{vk}) = \frac{1}{\sigma^{N_r} \sigma^{2N_r}} \exp\left(\frac{-\|y - \hat{H}x_{vk}\|_F^2}{\sigma^N}\right) \tag{9}$$

Receiver complexity

For simplicity, assume each frame contains only one code-word. Then for the conventional SM, in each frame, the detector computes $\hat{H}x_{vk}$ where x_{vk} is a single column vector with nonzero entries corresponding to antenna v and time slot k . Evaluating this gives a total of N_r real-valued multiplications. Additionally, $2N_r$ real-valued multiplications are necessary to compute the Frobenius norm. A total of MN_t different combinations for SM will be searched by an ML detector, and therefore, each SM's overall computational complexity is $C_{SM} = 6N_rN_tM$ (multiplication of real values). For the GASSM, this is the complexity in each of the time slots and for three antenna transmission, the complexity per frame becomes $C_{GASSM} = 18N_rN_tM$.

However, to achieve a given spectral efficiency, it is observed that the conventional SM computational complexity increases very rapidly compared to the GASSM. Table 1 shows the different modulation techniques, complexity expression of the receiver and the number of computations the receiver needs to detect a symbol are shown in Table 7. For the 5-bit and 7-bit GASSM, since the modulation technique uses BPSK, the number of multiplications is far much lower than that of the conventional SM. Since 6-GASSM utilizes 4-QAM transmission, the number of complex multiplications is relatively higher, as compared to BPSK transmissions. The values used for the computation of the complexities are, $N_r = 4$, $N_t = 2$ and $M = 4$ for conventional SM, $N_r = N_t = 3$ for the GASSM with GASSM-5 and GASSM-7 using BPSK and GASSM-6 using 4-QAM.

Table 7 Comparison of the complexity analysis for 3 time slots

Modulation	Complexity expression	Product
Conventional SM-3 bpcu	$6N_rN_tM$	192
GASSM-5 bpcu	$18N_rN_tM$	324
GASSM-6 bpcu	$18N_rN_tM$	648
GASSM-7 bpcu	$18N_rN_tM$	324

Error performance analysis

The error performance equations are derived based on the sample variance (SV) and mutual information (MI) criteria as derived in [29]. It is shown that the additional level of detection of the spatial information degrades the bit-error rate performance. We use the derived equation to obtain the bit error rate of the GASSM system as:

$$P_{GASSM} = \frac{P_{SIMO}}{b_e} \tag{10}$$

where b_e is the MA-SM system's bit error bit density.

SIMO SEP of the modulation domain from the Q-approximation

The symbol error rate (SER) expression can be obtained by estimating the symbol error rate for the SIMO system for the M -ary QAM [6] and approximating the outcome using the trapezoidal rule of the Q-approximation

$$P_{SIMO} = \frac{a}{c} \left[\frac{1}{2} \left(\frac{2}{b\rho + 2} \right)^{N_R} - \frac{a}{2} \left(\frac{1}{b\rho + 1} \right)^{N_R} \right] + \frac{a}{c} \left[(1 - b) \sum_{i=1}^{c-1} \left(\frac{\beta_i}{b\rho + \beta_i} \right)^{N_R} + \sum_{i=1}^{2c-1} \left(\frac{\beta_i}{b\rho + \beta_i} \right)^{N_R} \right] \tag{11}$$

where N_R denotes the number of receive antennas, ρ is the average SNR, $a = 1 - \frac{1}{M}$, $b = \frac{1}{M-1}$, $\beta_i = 2 \sin^2 \theta_i$, $\theta_i = \frac{i\pi}{4c}$ and $c = 10$ is the number of repetitions required for the expression to converge.

Sample variance criterion

As evaluated in [29], the process of determining the number of error components through sample variance can be outlined as follows:

Algorithm: Searching for joint space eigenvalue:

1. Obtain the matrix of the error distances in the detectors joined signal space;
2. Determine the covariance matrix from the matrix in step 1;
3. Correct the sample variance in the estimate of the population variance;
4. Obtain the largest eigenvalue for the joint space;
5. The eigenvalue in step 4 is used to represent the error data in the detector;
6. Add the covariance samples $I_c = \binom{N_a}{2}$ where N_a represents the multiple transmit chains.

Through this procedure, the authors have shown that the density of error through the SV criterion is obtained from

$$b_{e,SV} = \left(\frac{I_c}{\sqrt{N_t/M - 1}} \right) \tag{12}$$

where $b_{e,SV}$ is the density of bits in error due to average noise from a space of N_t transmit antennas, M is the modulation order and I_c is the covariance samples.

Mutual information (MI) criterion

In a similar manner, from [29], the expression for determining the BER through the mutual information can be outlined as follows:

Algorithm: Obtaining the density of bits in error through MI:

1. Using Fano’s inequality derive the mutual information for two random variables X and \hat{X} of the same alphabet α ;
2. Use the information in step 1 to obtain the mutual information lost between the spatial and the symbol variables;
3. Obtain the density of error using the MI criterion;
4. Add the covariance samples I_c .

For the MI criterion and MQAM modulation, it is shown that

$$b_{e,MI} = \left| \log_2 \left(\frac{I_c N_t}{M - 1} \right) \right| \tag{13}$$

The criterion for the selection of the optimal theoretic model that gives the smallest amount of error is chosen based on [29] and given by:

$$b_e = \min (b_{e,SV}, b_{e,MI}) \tag{14}$$

Therefore, the formulas in (10) can be utilized to derive the average bit error probability for the GASSM by substituting them in Eq. (10).

Secrecy rate analysis

For secrecy rate analysis, we employ the MIMO eavesdropper wiretap model shown in Fig. 2. Alice’s antenna conveys patterns of sequence as transmitted signal to the intended recipient Bob. However, another illegitimate user Eve is present with a means of intercepting the information on the intended channel. By applying Eq. (1) to the wiretap model,

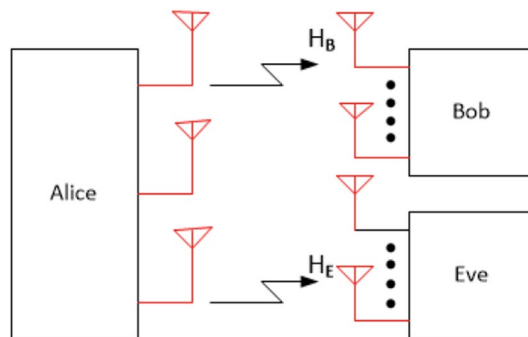


Fig. 2 GASSM Wiretap model

$$\begin{aligned} \mathbf{y} &= \mathbf{H}_B \mathbf{x} + \mathbf{n}_1 \\ \mathbf{z} &= \mathbf{H}_E \mathbf{x} + \mathbf{n}_2 \end{aligned} \tag{15}$$

where \mathbf{y} and \mathbf{z} are the legitimate and eavesdropper’s received signal vectors, respectively, with \mathbf{H}_B and \mathbf{H}_E being the corresponding channel matrices for Bob and Eve, respectively. \mathbf{n}_1 and \mathbf{n}_2 are the noise vectors for each of the channel matrices and the input signal vector is represented by \mathbf{x} .

Genuine receivers and eavesdroppers are assumed to be both familiar with their own channels. The secrecy rate measures how the information shared by an actual user, Bob, and an observer, Eve, differs. At different average SNR values, the expression of the secrecy capacity can be obtained. For a typical SIMO model, the feasible secrecy rate R_{simo} is expressed as:

$$R_{simo} = \max \{0, I(\mathbf{x}; \mathbf{y}|\mathbf{H}_b) - I(\mathbf{x}; \mathbf{z}|\mathbf{H}_e)\} \tag{16}$$

For a $N_r \times N_t$ channel, $H \sim CN(0, 1)$, the mutual information in Eq. (16) can be calculated using the formula:

$$I(\mathbf{x}; \mathbf{y}|\mathbf{H}_e) = \mathbb{E}_{\mathbb{H}} \left(\int_{\mathbf{y}} P_{\mathbf{X}\mathbf{Y}|\mathbf{H}}(x, y|\mathbf{H}) \times \log \frac{P_{\mathbf{X}\mathbf{Y}|\mathbf{H}}(x, y|\mathbf{H})}{P_{\mathbf{X}|\mathbf{H}}P_{\mathbf{Y}|\mathbf{H}(y|\mathbf{H})}} d\mathbf{y} \right) \tag{17}$$

where \mathbb{H} is the entropy function and the complex Gaussian distribution of the N_r -dimensional received signal has a conditional probability density function that is given by:

$$P_{\mathbf{Y}|\mathbf{X}\mathbf{H}}(y|x_m, \mathbf{H}) = \frac{1}{\pi^{N_r} \sigma_n^{2N_r}} \exp \left(-\frac{\|y - Hx_m\|_F^2}{\sigma_n^2} \right) \tag{18}$$

where $P_{\mathbf{Y}|\mathbf{X}\mathbf{H}}(y|x_m, \mathbf{H})$ is the PDF of \mathbf{Y} given \mathbf{X} and \mathbf{H} .

Alternatively, Eq. (16) in terms of the entropy $\mathbb{H}_e(y|x_m, H)$ where $m \in M$ can be written as:

$$\begin{aligned} I(\mathbf{x}; \mathbf{y}|\mathbf{H}_e) &= \mathbb{H}_e(y|x_m, H) - E_{\theta} [\mathbb{H}_e(y|\alpha_m, H)] \\ &= \beta + E_{\theta} [\mathbb{H}_e(y|\alpha_m, H)] \end{aligned} \tag{19}$$

$$\mathbb{H}_e(\mathbf{y}|x_m, H) = \sum_{x_m \in M} P(y|\alpha_m, H) \log_2 P(y|\alpha_m) \tag{20}$$

Secrecy rate from BER

By using Fano’s inequality

Table 8 Simulation parameters for Fig. 3

Parameter	Conventional SM			GASSM		
No. of transmit antennas, \mathbf{N}_t	4	4	4	3	3	3
Modulation order, \mathbf{M}	4	64	8	2	2	4
Spectral efficiency, \mathbf{bpcu}	4	8	5	7	5	6

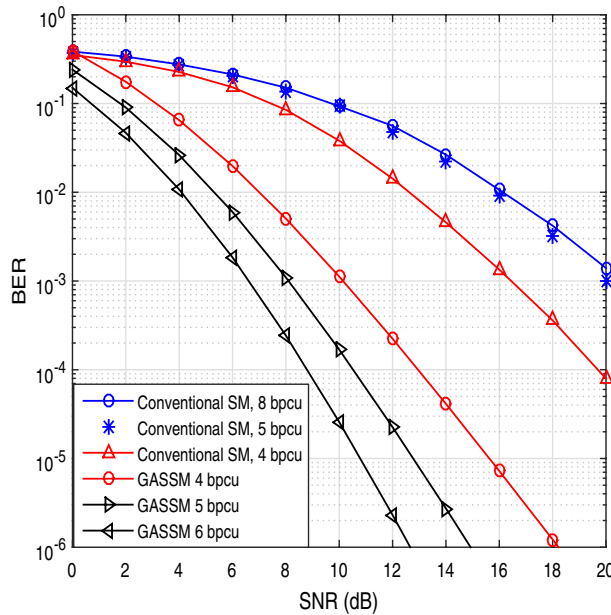


Fig. 3 Performance of GASSM and conventional SM under different spectral efficiencies

$$\begin{aligned}
 \mathbb{H}_E(\mathbf{X}|\hat{\mathbf{X}}) &\leq \mathbb{H}(e) + P(e) \log_2(|\chi| - 1) \\
 \mathbb{H}_e(\mathbf{X}|\hat{\mathbf{X}}) &\leq \mathbb{H}(e) + P(e) - [1 - P(e)] \log_2[1 - P(e)]
 \end{aligned}
 \tag{21}$$

where $P_e = P_{GASSM}$. By substituting Eq. (11) into (10) and (10) into (20), the expression for the achievable secrecy rate in (16) is determined.

Results and analysis

BER analysis

Table 8 shows the simulation parameters used to obtain Fig. 3. The parameters includes values of the transmit antenna N_t , the modulation order M , in rows one and two, respectively, and the resultant spectral efficiencies in row three for the conventional SM and the GASSM for each of the parameters. It is observed that for a given SNR, the BER performance of the GASSM is better than that of the conventional SM, albeit at a lower spectral efficiency, a feature which is desirable in applications where reliability is prioritized.

In the case of GASSM, bipolar phase shift keying (BPSK) used with three antennas achieves spectral efficiency of 7 bpcu, without having to use higher-order modulation schemes. The same observation is made for the case of a spectral efficiency of 5 and 6 bpcu for the conventional SM and the GASSM, respectively. A simpler arrangement of modulation order of 4, in this case, 4-QAM and 3 transmitting antennas gives the spectral efficiency which is almost equal to that of conventional SM with 4 antennas and the same modulation order.

For the GASSM, since each time slot contains a unique information, the spectral efficiency is not affected by the use of the 3 time slots.

The performance of the GASSM in Rayleigh-correlated channels with various receive antenna numbers is presented and discussed in Fig. 4. The case of $N_r = 3, 4$ and 5 are

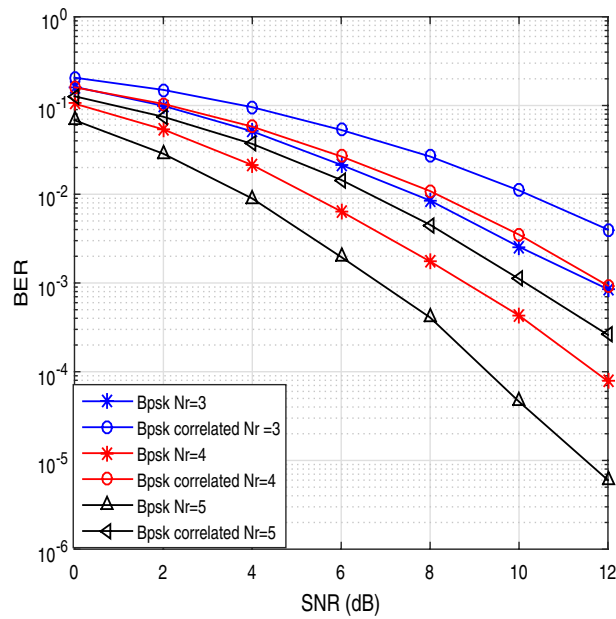


Fig. 4 Performance of 5 bit-GASSM under correlated channel with distance of separation of 0.2λ for $N_R = 3, 4,$ and 5

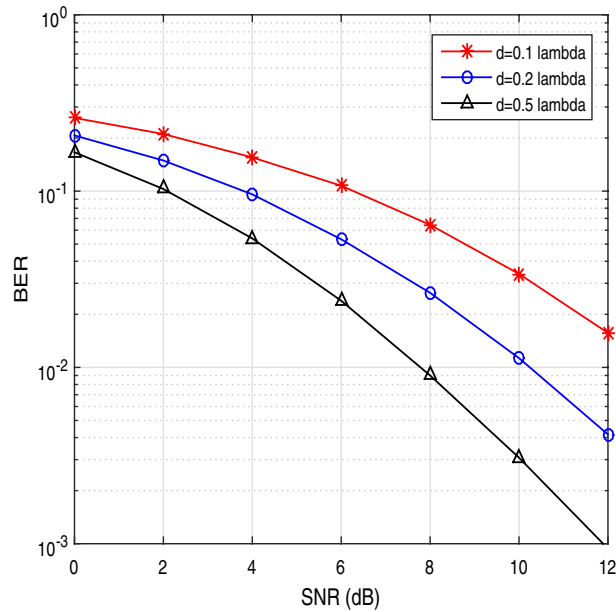


Fig. 5 Performance of 5 bit-GASSM under Rayleigh-correlated channel with $d = 0.1\lambda, 0.2\lambda, 0.5\lambda$ and $N_R = 3$.

considered. By using antenna separation distance of $d = 0.2\lambda$, and Eq. (5), a correlation matrix Σ is obtained to be:

$$\Sigma = \begin{pmatrix} 1 & 0.6425 & -0.550 \\ 0.6425 & 1 & 0.6425 \\ -0.550 & 0.6425 & 1 \end{pmatrix} \tag{22}$$

The correlated channel with BPSK modulation and the given number of receive antennas, N_r , and the uncorrelated values denoted by BPSK N_r and BPSK-correlated N_r , respectively, are compared in the graph. It is observed that the performance improves with the increase in the number of receive antennas. For each case, correlation degrades the performance of the channel, all factors remaining constant. For both the correlated and the uncorrelated cases $N_r = 3, 4, 5$. are considered.

In Fig. 5, the number of receive antennas is kept at $N_r = 3$ with $d = 0.1\lambda, 0.2\lambda$ and 0.5λ . The correlation coefficient matrix is determined for each case. The graph shows that performance degrades more rapidly the closer the antenna spacing is. This degradation is attributed to the significant cross correlation between adjacent signals with the decrease in the distant of separation.

The theory and simulation results of the 6 bit GASSM are presented in Fig. 6. The SV and MI criteria of evaluating the theoretical performance are discussed in “Sample variance criterion” and “Mutual information (MI) criterion” sections as a new methodology for evaluating the BER. The graphs shows a tight matching between the theoretical and the simulated results. The case of transmitting antenna of $N_t = 3$ by $N_r = 4, 5$ and 6 is presented.

It is evident that the performance improves with the number of receive antennas, and there is an exact match between the theory and simulation for the case of SV and not MI. The mismatch between the MI criterion and the QAM performance has been observed, and we propose that only the SV theoretical approach be applied for the QAM case. This applies as well to the performance of the 7-bit GASSM presented in Fig. 7

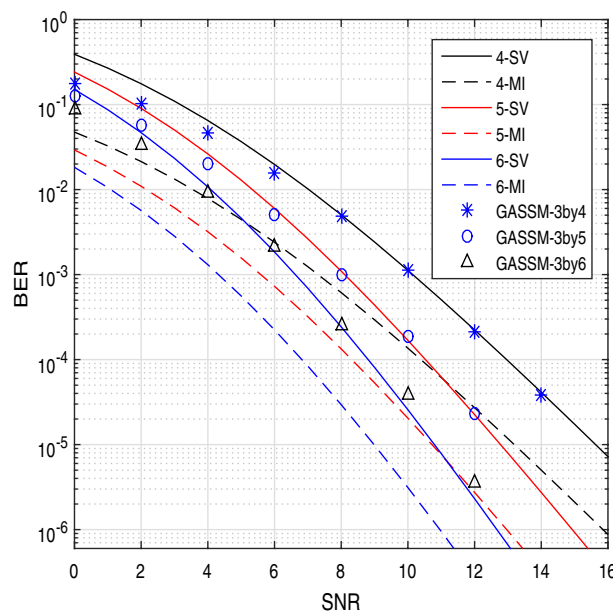


Fig. 6 BER performance of 6-bit GASSM-3-by-Nr, 4 QAM

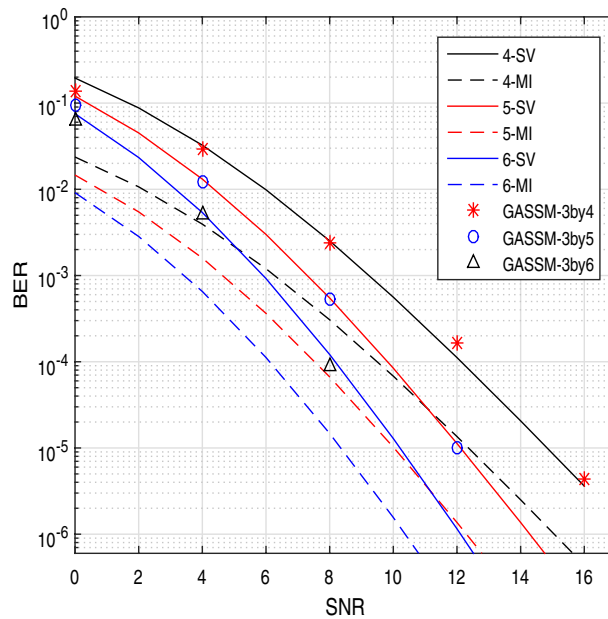


Fig. 7 BER performance of 7-bit GASSM 3 – by – N_r BPSK

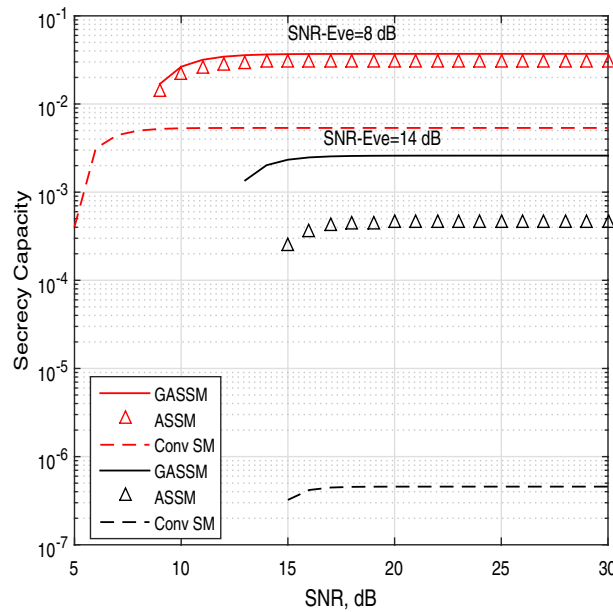


Fig. 8 Secrecy capacity: GASSM, ASSM and conventional SM

Secrecy rate analysis

The lower the SNR between the eavesdropper (Eve) and the transmitter, the more secure the system is. This is because the channel is more noisy and the eavesdropper cannot intercept much information. This is shown in Fig. 9 by comparing the case of the SNR of 8 dB and 14 dB. The findings demonstrate that the secrecy capacity associated with an SNR of 8 dB is greater than the secrecy capacity associated with an SNR of 14 dB. For the

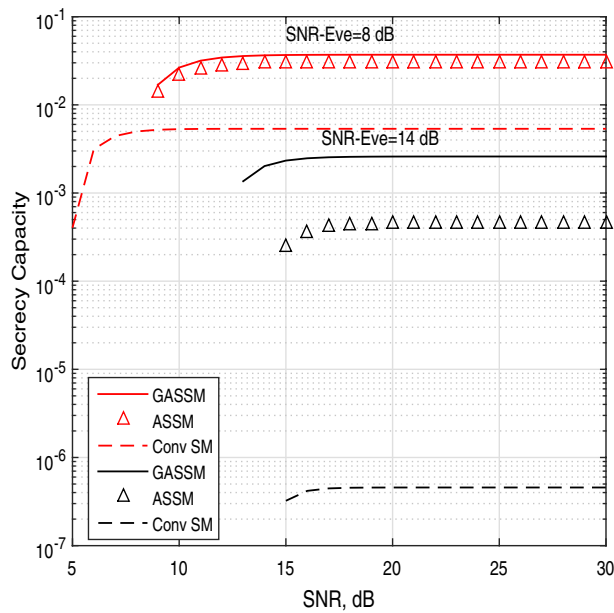


Fig. 9 Secrecy capacity: 7-bit GASSK and 6-bit 4-QAM

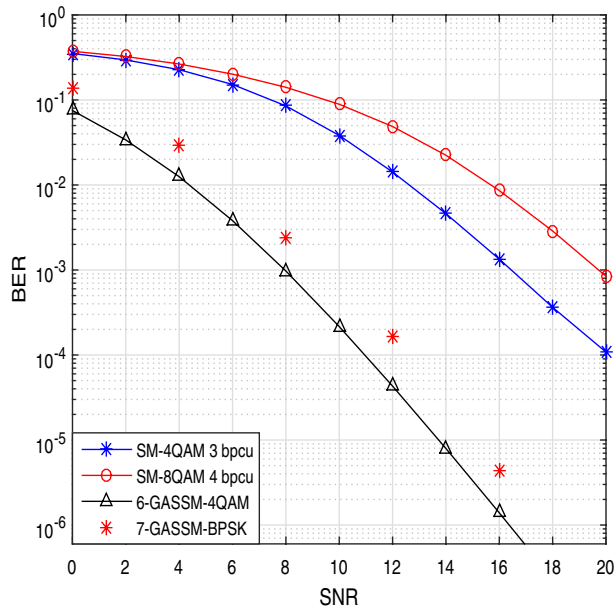


Fig. 10 Comparison of Data Rates: SM and GASSM

SNR of 8 dB, it is observed that the secrecy capacity is highest in GASSM, followed by ASSM and finally SM. The same order is observed for the case of the SNR of 14 dB.

Table 9 Comparison of symbol rate

Modulation	Bits per symbol	Symbol rate
SM 4-QAM	4	$\frac{1}{4}$
6 GASSM 4-QAM	6	$\frac{2}{6}$
7 GASSM BPSK	7	$\frac{3}{7}$

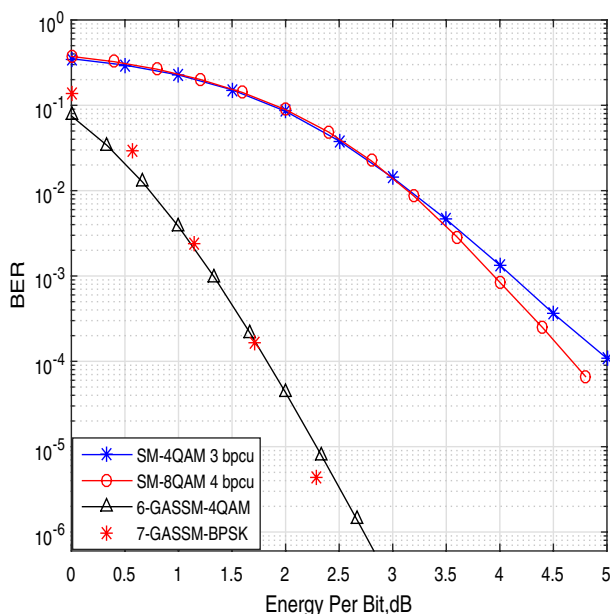


Fig. 11 Comparisons of energy per unit bit

Figure 9 shows the secrecy capacity of 7-bit GASSM and the 6-bit GASSM under an SNR of 8 dB. The 7-bit GASSM uses the more robust but predictable BPSK modulation. As expected to decipher, a 7-bit pattern is more complex than to decipher a 6-bit pattern. Consequently, the secrecy capacity of the 7 bit GASSM is higher than that of the 6-bit GASSM with 4QAM modulation.

Figures 8 and 9 demonstrate how the secrecy capacity varies depending on the modulation type and the SNR of the channel between the eavesdropper and the information source. On comparison of the graphs, it is shown that for a given SNR, GASSM has a higher secrecy capacity than the ASSM and the SM. However, within the GASSM, the longer the length of the code, the higher the secrecy capacity.

Data rate analysis

Table 9 shows modulation type, the corresponding bits per symbol and the symbol rate. For the SM-4 QAM, 1 symbol represents 4 bits, giving a symbol rate of $\frac{1}{4}$. For the 7-bit GASSM, three symbols (transmitted over three consecutive time slots) represent 7 bits, giving a symbol rate of $\frac{3}{7}$. From the table, it is observed that the symbol rate increases, the highest being for the 7 bit GASSM BPSK as further illustrated in Fig. 10.

Table 10 Comparison of the important parameters

Modulation	Energy per bit at BER of 10^{-3}	Secrecy capacity SNR of 8dB for Eve	BER at channel Utilization of 4bpcu	Receiver Complexity
GASSM	1.4	10^{-2}	10^{-3}	$6N_r N_t M$
SM	4.0	10^{-3}	10^{-1}	$18N_r N_t M$

Bit-energy efficiency analysis

Figure 11 shows the performance of the GASSM and SM systems by considering the energy expended per bit. From the figure, it is inferred that a given BER is obtained by a low energy per unit bit with the GASSM schemes than with the SM scheme. Energy efficiency is important in industrial applications and in future generation networks. In devices such as field programmable gate array (FPGA) and application-specific integrated circuit (ASIC), the increased miniaturization of the transistors results in high component density, leading to increased power consumption and added cost in manufacturing as special materials have to be used in modified packaging and sometimes cooling mechanisms. A bit-energy-efficient scheme will lead to reduced manufacturing cost of these devices as the expected power to be handled is reduced. Energy-efficient bit transmission forms part of the high power amplifier (HPA) optimization strategy, especially in the linear region of operation. For mobile devices, energy efficiency leads to increased battery life, which is a key requirement in today's emerging networks.

Comparison of important parameters

Table 10 shows a summary of selected parameters of GASSM against the SM. At a BER of 10^{-3} , the energy per bit for GASSM and SM is 1.4 and 4, respectively. Similarly, at an SNR of 8dB between Eve and Alice, the GASSM is 10 times as secure as the SM. At a performance of 4 bpcu, the BER of the GASSM is better than that of the SM. However, the receiver of the GASSM is more complex than that of the SM.

Conclusion

The reliability, data rate and secrecy capacity of the ASSM and conventional SM are improved by the proposed GASSM communication model. In scenarios where both spectral efficiency and high security capacity are required, comparisons of data rates and secrecy capacity demonstrate that GASSM is a suitable candidate for next-generation networks. Further, GASSM offers a higher efficiency per bit transmission, a key requirement in future generation networks.

Acknowledgements

Not applicable.

Author contributions

The following approximates each of the authors' contributions: JAO did simulations and development of mathematical framework for the proposed communication system. PA was the holder of the patent describing this novel communication system. Supervision of the accuracy of the simulations and the mathematical framework. Verification of the obtained results. VO done the guidance on the research direction and verification of the accuracy of the results obtained. All the authors proofread and corrected the manuscript before the final submission.

Funding

There is no funding.

Availability of data and materials

Not applicable. The research is done through simulations and development of mathematical framework.

Declarations**Competing interests**

There are no competing interests.

Received: 25 August 2023 Accepted: 28 December 2023

Published online: 29 January 2024

References

1. Yu P, Huang F (2022) Spatial index modulation with the combination of both antenna indexes and two constellations. *IEEE Access* 10:133778–133788. <https://doi.org/10.1109/ACCESS.2022.3230838>
2. Jeganathan J, Ghrayeb A, Szczecinski L, Ceron A (2009) Space shift keying modulation for MIMO channels. *IEEE Trans Wirel Commun* 8(7):3692–3703. <https://doi.org/10.1109/TWC.2009.080910>
3. Jeganathan J, Ghrayeb A, Szczecinski L (2008) Generalized space shift keying modulation for MIMO channels, pp 1–5. <https://doi.org/10.1109/PIMRC.2008.4699782>
4. Mesleh R, Haas H, Ahn CW, Yun S (2006) Spatial modulation—a new low complexity spectral efficiency enhancing technique, pp 1–5. <https://doi.org/10.1109/CHINACOM.2006.344658>
5. Gudla VV, Gamini S, Kumaravelu VB, Soria FRC (2022) Performance evaluation of fully quadrature spatial modulation under various channel fading scenarios. In: 2022 2nd international conference on artificial intelligence and signal processing (AISP), pp 1–5. <https://doi.org/10.1109/AISP53593.2022.9760567>
6. Mesleh R, Ikki SS, Aggoune HM (2015) Quadrature spatial modulation. *IEEE Trans Veh Technol* 64:2738–2742. <https://doi.org/10.1109/TVT.2014.2344036>
7. Akuon PO, Xu H (2022) Performance of ma-spatial modulation: information theoretic criteria over correlated Rayleigh channel. *IET Commun* 10(9):1071–1079. <https://doi.org/10.1049/iet-com.2015.0822>
8. Li J, Dang S, Yan Y, Peng Y, Al-Rubaye S, Tsourdos A (2021) Generalized quadrature spatial modulation and its application to vehicular networks with NOMA. *IEEE Trans Intell Transp Syst* 22(7):4030–4039. <https://doi.org/10.1109/TITS.2020.3006482>
9. Ozden BA, Aydin E, Cogen F (2023) Code index modulation-aided spatial media-based modulation system for future wireless networks. *IEEE Syst J* 17:3762–3770. <https://doi.org/10.1109/JSYST.2022.3230775>
10. Kumar BN, Pal D, Bandyopadhyay AK, Koley C (2023) Spectral efficiency analysis using underlay cognitive radio transmission over Rician fading channels. In: 2023 4th international conference on computing and communication systems (ICCS), pp 1–5. <https://doi.org/10.1109/ICCS58314.2023.10127544>
11. Yadav P, John BB, Dutta A, Vasavada Y (2023) A spectrally efficient MIMO system with sparse matrix precoding. In: 2023 IEEE wireless antenna and microwave symposium (WAMS), pp 1–5. <https://doi.org/10.1109/WAMS57261.2023.10242919>
12. Akuon PO, Xu H (2022) Layered baud-space modulation: flexible SM scheme under transmit and receive correlation. *IET Commun* 16(9):1797–1806. <https://doi.org/10.1049/cmu2.1242>
13. Obadha JA, Akuon PO, Oduol VK (2022) Secrecy and BER analysis of antenna sequence spatial modulation: an information theoretic approach. *IET Commun* 16(15):1815–1825. <https://doi.org/10.1049/10.1049/cmu.12434>
14. Akuon PAM (2017) Systems and Methods for Communications. Patent. W02018083601 (Nov 2017, [online] Available). <https://patentscope.wipo.int/search>
15. Akuon P, Xu H (2015) A multiple rank modulation system. SA. <https://patents.google.com/patent/WO2017037562A1/en>
16. Obadha JA, Akuon PO, Kalecha VO (2019) BER of antenna code sequence modulation (ACSM) and analysis under repetition. In: 2019 IEEE AFRICON, pp 1–5. <https://doi.org/10.1109/AFRICON46755.2019.9133982>
17. Obadha JA, Akuon PO, Kalecha VO (2021) BER performance of antenna sequence modulation (ASM). In: 2021 IEEE AFRICON, pp 1–6. <https://doi.org/10.1109/AFRICON51333.2021.9570995>
18. Nyawade A, Akuon PO, Xu H, Kalecha VO (2019) Spatial MIMO rank modulation. In: 2019 IEEE AFRICON, pp 1–6. <https://doi.org/10.1109/AFRICON46755.2019.9134052>
19. Nyanjom JO, Akuon PO, Oduol VK (2021) BER performance of frequency-coded multiple rank modulation, pp 1–5. <https://doi.org/10.1109/AFRICON51333.2021.9571003>
20. Faris AA, Akuon PO, Kalecha VO (2021) BER performance of SSK sequence modulation, pp 1–6. <https://doi.org/10.1109/AFRICON51333.2021.9570926>
21. Shannon C (1949) Communication theory of the secrecy systems. *Bell Syst Tech J* 28(4):656–715
22. Wyner AD (1940) the wiretap channel bell. *Bell Syst Tech J* 54(8):1355–1387
23. Bassily R, Ekrem E, He X, Tekin E, Xie J, Bloch MR, Uluks S, Yener A (2013) Cooperative security at the physical layer: a summary of recent advances. *IEEE Signal Process Mag* 30(5):16–28. <https://doi.org/10.1109/MSP.2013.2260875>
24. Mheich Z, Alberge F, Duhamel P (2015) Achievable secrecy rates for the broadcast channel with confidential message and finite constellation inputs. *IEEE Trans Commun* 63(1):195–205. <https://doi.org/10.1109/TCOMM.2014.2374604>
25. Nazzal T, Mukhtar H (2021) Evaluation of key-based physical layer security systems. In: 2021 4th international conference on signal processing and information security (ICSPIS), pp 84–87. <https://doi.org/10.1109/ICSPIS53734.2021.9652423>

26. Etemadi Tajbakhsh S, Coon JP, Chen G (2018) Network coding for physical layer secrecy. *IEEE Wirel Commun Lett* 7(4):642–645. <https://doi.org/10.1109/LWC.2018.2806452>
27. Hu Q, Huang N, Gong C (2023) Superposition modulation for physical layer security in water-to-air visible light communication systems. *J Lightw Technol* 41:2976–2990. <https://doi.org/10.1109/JLT.2023.3240180>
28. Hoseini SA, Bouhafaf F, den Hartog F (2022) A practical implementation of physical layer security in wireless networks, pp 1–4. <https://doi.org/10.1109/CCNC49033.2022.9700672>
29. Akuon PO, Xu H (2022) Optimal error analysis of receive diversity schemes on arbitrarily correlated Rayleigh fading channels. *IET Commun* 16(15):1815–1825. <https://doi.org/10.1049/10.1049/cmu.1242>
30. Parida P, Dhillon HS (2023) Cell-free massive MIMO with finite fronthaul capacity: a stochastic geometry perspective. *IEEE Trans Wirel Commun* 22(3):1555–1572. <https://doi.org/10.1109/TWC.2022.3205349>
31. Yu J, Yang J, Wang S, Cai Y, Liu J (2023) Low-complexity beam selection algorithms based on SVD for mmWave massive MIMO systems. *IEEE Commun Lett* 27:2436–2440. <https://doi.org/10.1109/LCOMM.2023.3292126>
32. Tania MT, Ibrahim M, Hossen MS, Badrudduza ASM, Kundu MK (2022) Combined impacts of co-channel interference and correlation on secrecy performance over $\kappa - \mu$ shadowed fading channel, pp 1–6 (2022). <https://doi.org/10.1109/ICAEES54957.2022.9836431>

Publisher's Note

Springer Nature remains neutral with regard to jurisdictional claims in published maps and institutional affiliations.

Joseph Abok Obadha is a Ph.D. researcher in the Wireless research group, department of Electrical and Information Engineering, University of Nairobi. Prof. Vitalis Oduol and Dr. Peter Akuon are senior lecturers and researchers in the same department. They hold several patents in Wireless in novel Communication methods